Experimed 2024; 14(3): 161-173

ORIGINAL ARTICLE

DOI: 10.26650/experimed.1491074

Epigenetic Signatures in Ovarian Cancer to Determine Potential Diagnostic/Prognostic Biomarkers

Tugce Senturk Kirmizitas [1,2], Servet Tunoglu[3], Jean Helmijr[2], Samet Topuz[4], Maurice Jansen[2], Tuba Gunel[4]

[1]Department of Molecular Biology and Genetics, Faculty of Science, Istanbul University, Istanbul, Turkiye
[2]Department of Medical Oncology, University Medical Center Rotterdam, Rotterdam, The Netherlands
[3]Department of Molecular Medicine, Aziz Sancar Institue of Experimental Medicine, Istanbul University, Istanbul, Turkiye
[4]Department of Obstetrics and Gynecology, Istanbul Medical Faculty, Istanbul University, Istanbul, Turkiye

ORCID ID: T.S.K. 0000-0001-6235-251X; S.T. 0000-0001-7625-7425; J.H. 0000-0003-0983-6296; S.Topuz 0000-0002-9069-0185; M.J. 0000-0003-1258-9804; T.G. 0000-0003-3514-5210

Cite this article as: Senturk Kirmizitas T, Tunoglu S, Helmijr, J, Topuz S, Jansen M, Gunel T. Epigenetic signatures in ovarian cancer to determine potential diagnostic/prognostic biomarkers. Experimed 2024; 14(3): 161-173.

ABSTRACT

Objective: Identification of methylation patterns in cell-free DNA (cfDNA) provides a non-invasive methodology for discovering critical biomarkers that facilitate detection and prognostic evaluation of ovarian cancer (OC). This study explored the epigenetic landscape of OC by examining the DNA methylation patterns of cfDNA.

Materials and Methods: Plasma samples from 5 OC patients and 5 healthy blood donors (HBDs) were processed for cfDNA isolation and methylated DNA immunoprecipitation, followed by next-generation sequencing and bioinformatics analysis to identify differentially methylated regions (DMRs) and genes (DMGs). Integration with The Cancer Genome Atlas (TCGA) data identified differentially expressed genes (DEGs) for functional analysis.

Results: The analysis revealed significant alterations in DNA methylation patterns, with 62 hypermethylated and 2 hypomethylated DMRs in OC compared with HBDs. Hierarchical clustering revealed distinct methylation patterns between OC and HBDs. Integrative analysis identified 18 genes with overlapping methylation and expression changes in OC and a negative correlation between methylation and expression levels ($p<0.05$). Ten genes exhibited a hypermethylation-downregulation pattern, indicating a suppressive role, whereas eight showed hypermethylation-upregulation. Survival analysis of OC data from TCGA highlighted *B3GNT3* ($p=0.04$) and *LRP1B* ($p=0.053$) as promising prognostic markers.

Conclusion: Our study revealed an intricate relationship between DNA methylation alterations and gene expression dysregulation in ovarian cancer. We found that hypermethylation of *B3GNT3* was correlated with its upregulation and poor survival outcomes, whereas hypermethylation of *LRP1B* pointed to its role as a tumor suppressor gene.

Keywords: Epithelial ovarian cancer, methylation, epigenomics, liquid biopsy, cfDNA

INTRODUCTION

Ovarian cancer (OC) is a highly prevalent and deadly cancer that affects female reproductive organs, with an increasing incidence worldwide (1). It is currently the second most common cancer of the female reproductive system. The most prevalent form, epithelial ovarian cancer (EOC), accounts for 85%–90% of ovarian tumors. OC spreads through direct extension, intra-abdominal seeding, and lymphatic routes, with advanced stages often involving peritoneal metastases, resulting in high mortality and poor prognosis (2). Treatment for advanced OC usually involves surgical tumor removal

Corresponding Author: Tugce Senturk Kirmizitas **E-mail:** tugce.senturk.12@gmail.com
Submitted: 28.05.2024 **Revision Requested:** 16.07.2024 **Last Revision Received:** 06.08.2024 **Accepted:** 06.08.2024

and platinum-based chemotherapy (3). Despite treatment advancements, the prognosis remains poor, and OC has the highest mortality rate among gynaecological cancers. OC is typically asymptomatic in the early stages, and the absence of reliable biomarkers for early detection often leads to diagnosis at the late stage, making it more difficult to treat and resulting in worse outcomes. Thus, the development and validation of effective detection and prognostic biomarkers are essential for improving early diagnosis and survival rates for patients (4).

Recent studies have highlighted the crucial role of epigenetic modifications in the development and progression of OC (5-8). Epigenetic changes, particularly DNA methylation, are emerging as promising non-invasive biomarkers for the early detection and monitoring of OC. DNA methylation, which involves addition of methyl groups to DNA promoter regions, regulates gene expression and is mediated by a complex network of enzymes, co-factors, and regulatory proteins (9). Tumor cells often exhibit abnormal DNA methylation at the promoters of tumor-suppressor genes and oncogenes, disrupting key biological processes such as cell proliferation, cell cycle regulation, and apoptosis (9, 10). This disruption is associated with the development and metastasis of OC. In parallel, liquid biopsy has emerged as a promising approach in oncology, enabling non-invasive detection of tumor-derived material from various bodily fluids (11, 12). Cell-free DNA (cfDNA) holds particular significance among the analytes examined, as its aberrant DNA methylation profiles mirror tumorigenesis and cancer progression (13). Despite the challenges associated with low levels of methylated cfDNA, cfDNA methylation analysis shows potential as a biomarker for the diagnose and treatment of ovarian cancer (2, 14).

We investigated the epigenetic landscape of OC by analyzing DNA methylation patterns in cfDNA from plasma samples of OC patients and healthy blood donors (HBDs). We used methylated DNA immunoprecipitation (MeDIP) followed by next-generation sequencing (NGS) to identify differentially methylated regions (DMRs) and genes (DMGs). Additionally, we integrated our findings with differentially expressed genes (DEGs) from The Cancer Genome Atlas (TCGA) dataset to identify genes with concurrent methylation and expression changes, thereby providing a more comprehensive understanding of the epigenetic regulation in OC.

The present study underscores the intricate relationship between DNA methylation alterations and gene expression dysregulation in OC. Our findings contribute to the growing body of knowledge regarding the epigenetic mechanisms driving OC and highlight potential biomarkers and therapeutic targets for improving patient outcomes.

MATERIALS AND METHODS

Sample Collection

To identify DMRs in cfDNA from OC patients compared with healthy individuals, we utilized samples from 5 OC patients and 5 HBDs. The clinical and demographic characteristics of the patient samples involved in this study are presented in Table 1. Blood samples were obtained from serous adenocarcinoma from OC patients prior to surgery, who had not received any treatment. In the control group called HBDs, individuals with no history of cancer and without other diseases, such as diabetes, endometriosis, or hypertension, were included.

Table 1. Clinical and demographic characteristics of OC samples

Characteristics	OC (n=5)
Age Mean (Range)	54.4 (35-75)
CA125 Mean (Range)	859 (62-1754)
Types	
Primer Serous	5
FIGO Stage	
Stage 3A	1
Stage 3C	4
Recurrence	
Yes	0
No	3
Unknown	2
Lymphatic Invasion	
Yes	4
No	0
Unknown	1
Family History	
Yes	1
No	3
Unknown	1

Peripheral blood samples were collected in 10 mL EDTA tubes from individuals meeting the inclusion and exclusion criteria of the study. Using the cold chain method, these samples were transported to the Molecular Biology and Genetics Department of Istanbul University within 4 h. Samples were centrifuged at 600 g for 10 min at 4°C, followed by a second centrifugation at 14.000 g for 10 min at 4°C. Plasma was transferred to 1.5 mL cryotubes and stored at -80°C until cfDNA isolation. This study was approved in 2020 by Istanbul University, Istanbul Faculty of Medicine Clinical Research Ethics Committee under file number 1451. All participants provided voluntary informed consent by completing the consent forms after receiving detailed information.

Table 2. Summary of identified DMRs

DMR ID	Name	Chromosome	Start	End	Log2 Fold Change	p value
DMR1	*PDZD7*	chr10	1.03E+08	1.03E+08	4.047	0.0485
DMR2	*snoU13*	chr11	1.23E+08	1.23E+08	4.360	0.0492
DMR3	*PRDM11*	chr11	45114563	45116563	3.875	0.0405
DMR4	*AX747537*	chr11	880475	882475	3.495	0.0444
DMR5	*NOX4*	chr11	89056521	89058521	4.819	0.0156
DMR6	*7SK*	chr12	1.15E+08	1.15E+08	5.546	0.0062
DMR7	*CAPRIN2*	chr12	30880312	30882312	4.010	0.0493
DMR8	*ATN1*	chr12	7036479	7038479	4.820	0.0126
DMR9	*POU5F1P3*	chr12	8285945	8287945	6.275	0.0021
DMR10	*ZFHX2*	chr14	23989063	23991063	3.796	0.0225
DMR11	*KIAA0586*	chr14	58905398	58907398	5.229	0.0041
DMR12	*PPCDC*	chr15	75314926	75316926	6.473	0.0018
DMR13	*ZNF774*	chr15	90894476	90896476	3.443	0.0487
DMR14	*MCTP2*	chr15	94840429	94842429	4.333	0.0191
DMR15	*NR2F2*	chr15	96873110	96875110	4.493	0.0234
DMR16	*DQ585716*	chr15	97323965	97325965	4.530	0.0141
DMR17	*TEKT5*	chr16	10720360	10722360	4.247	0.0236
DMR18	*TMC5*	chr16	19428017	19430017	4.174	0.0127
DMR19	*DYNC1LI2*	chr16	66753798	66755798	4.443	0.0279
DMR20	*BX537921*	chr16	8739037	8741037	8.220	0.0001
DMR21	*RP11-744K17.9*	chr17	21903061	21905061	2.733	0.0359
DMR22	*LYRM9*	chr17	26204339	26206339	4.942	0.0234
DMR23	*RP11-647F2.2*	chr17	72298777	72300777	5.677	0.0101
DMR24	*SECTM1*	chr17	80277899	80279899	3.640	0.0359
DMR25	*MC5R*	chr18	13824542	13826542	-5.334	0.0160
DMR26	*PRDX2*	chr19	12906633	12908633	4.601	0.0229
DMR27	*NOTCH3*	chr19	15287335	15289335	3.812	0.0473
DMR28	*B3GNT3*	chr19	17904918	17906918	4.022	0.0389
DMR29	*LINC01224*	chr19	23581035	23583035	4.373	0.0292
DMR30	*PRODH2*	chr19	36289891	36291891	4.090	0.0339
DMR31	*CCER2*	chr19	39398619	39400619	4.632	0.0209
DMR32	*ZNF574*	chr19	42571628	42573628	4.469	0.0262
DMR33	*PTGIR*	chr19	47122724	47124724	3.825	0.0445

DMR34	*ZNF358*	chr19	7583128	7585128	3.674	0.0349
DMR35	*FMO5*	chr1	1.47E+08	1.47E+08	4.349	0.0320
DMR36	*S100A16*	chr1	1.54E+08	1.54E+08	3.405	0.0481
DMR37	*RP11-144L1.4*	chr1	1.58E+08	1.58E+08	3.953	0.0374
DMR38	*TRNA_Gly*	chr1	17052779	17054779	3.877	0.0118
DMR39	*TAS1R2*	chr1	19165092	19167092	4.081	0.0454
DMR40	*FCAMR*	chr1	2.07E+08	2.07E+08	4.695	0.0187
DMR41	*TRNA_Glu*	*chr1*	*2.49E+08*	*2.49E+08*	*4.613*	*0.0366*
DMR42	*LRP8*	*chr1*	*53715361*	53717361	4.423	0.0149
DMR43	*ZBTB46-AS1*	*chr20*	*62438441*	*62440441*	*4.134*	*0.0291*
DMR44	*LINC01548*	*chr21*	*34536775*	34538775	5.074	0.0047
DMR45	*CCDC74B-AS1*	*chr2*	*1.31E+08*	*1.31E+08*	*3.800*	*0.0286*
DMR46	*LRP1B*	*chr2*	*1.42E+08*	1.42E+08	4.373	0.0292
DMR47	*CD28*	*chr2*	*2.05E+08*	*2.05E+08*	*3.848*	*0.0443*
DMR48	*CXCR2P1*	*chr2*	*2.19E+08*	2.19E+08	4.560	0.0391
DMR49	*CCDC88A*	*chr2*	*55560229*	*55562229*	*4.529*	*0.0260*
DMR50	*LINC02049*	*chr3*	*1.21E+08*	1.21E+08	4.815	0.0075
DMR51	*FBXL21*	*chr5*	*1.35E+08*	*1.35E+08*	*4.745*	*0.0147*
DMR52	*RN7SL295P*	*chr5*	*1.6E+08*	1.6E+08	5.323	0.0079
DMR53	*WWC1*	*chr5*	*1.68E+08*	*1.68E+08*	*3.975*	*0.0385*
DMR54	*UIMC1*	*chr5*	*1.76E+08*	1.76E+08	4.694	0.0191
DMR55	*AX747985*	*chr5*	*1.79E+08*	*1.79E+08*	*4.473*	*0.0109*
DMR56	*MIR340*	*chr5*	*1.79E+08*	1.79E+08	4.629	0.0077
DMR57	*TRNA_Ser*	*chr6*	*27508553*	*27510553*	*4.376*	*0.0236*
DMR58	*MIR4641*	*chr6*	*41565460*	41567460	4.838	0.0074
DMR59	*EXOC4*	*chr7*	*1.34E+08*	*1.34E+08*	*5.972*	*0.0066*
DMR60	*SPDYE1*	*chr7*	*44039488*	44041488	4.853	0.0076
DMR61	*RNU6-229P*	*chr7*	*68865187*	*68867187*	*4.499*	*0.0413*
DMR62	*TG*	*chr8*	*1.34E+08*	1.34E+08	4.594	0.0110
DMR63	*RP11-115J16.1*	*chr8*	*9181560*	*9183560*	*4.215*	*0.0318*
DMR64	*MIR3134*	*chr9*	*1.15E+08*	1.15E+08	-5.190	0.0205

Summary of 64 statistically significant DMRs identified using the h19 reference genome. Each DMR was assigned a unique DMR ID ranging from 1 to 64. DMRs were identified based on their chromosomal locations, represented by the "Chromosome", "Start", and "End" columns. The statistical significance of each DMR is indicated by the calculated p value and log2 fold change, which were computed using the DESeq2 methodology. DMR: Differentially methylated region.

Table 3. Genes with overlapping methylation and expression patterns in OC

Overlapped DMG-DEG			CfMEDIP DMG		TCGA DEG	
Symbol	**Name**	**Called**	**Fold Change**	**p value**	**Fold Change**	**p value**
PRDM11	PR/SET domain 11	Hyper-Down	3.874	0.0493	-1.081	8.04E-31
CAPRIN2	C family member 2	Hyper-Down	4.009	0.0126	-2.246	8.97E-96
ATN1	Atropine 1	Hyper-Down	4.820	0.0020	-1.111	5.79E-24
POU5F1P3	POU class 5 homeobox 1 pseudogene 3	Hyper-Down	6.275	0.0234	-1.438	1.25E-179
NR2F2	Nuclear receptor subfamily 2 group F member 2	Hyper-Down	4.492	0.0126	-3.255	2.59E-106
TMC5	Transmembrane channel like 5	Hyper-Up	4.174	0.0278	1.38	2.33E-31
DYNC1LI2	Dynein cytoplasmic 1 light intermediate chain 2	Hyper-Down	4.442	0.0233	-1.598	9.79E-46
LYRM9	YR motif containing 9	Hyper-Down	4.941	0.0358	-2.219	1.39E-98
SECTM1	Secreted and transmembrane protein 1	Hyper-Up	3.639	0.0472	1.837	2.44E-19
NOTCH3	Notch receptor 3	Hyper-Up	3.812	0.0389	1.407	1.51E-13
B3GNT3	Beta-1,3-N-acetylglucosaminyltransferase 3	Hyper-Up	4.021	0.02912	3.373	6.70E-66
LINC01224	Long intergenic non-protein-coding RNA 1224	Hyper-Up	4.373	0.03203	2.348	6.18E-72
FMO5	Flavin containing monooxygenase 5	Hyper-Down	4.349	0.04812	-1.071	3.61E-59
S100A16	S100 calcium binding protein A16	Hyper-Up	3.404	0.01485	1.236	3.16E-17
LRP8	LDL receptor-related protein 8	Hyper-Up	4.423	0.02604	1.594	4.91E-34
CCDC88A	Coiled-coil domain containing 88A	Hyper-Down	4.528	0.03853	-1.23	3.43E-35
WWC1	WW and C2 domain containing 1	Hyper-Up	3.974	0.01912	4.036	7.61E-154
UIMC1	Ubiquitin interaction motif containing 1	Hyper-Down	4.693	0.02923	-1.982	3.34E-134

Log2 Fold Change (Log2FC) values represent differences in DNA methylation (cfMEDIP) and gene expression (TCGA mRNA) between OC and HBD. Positive Log2FC values denote hypermethylation in cfMEDIP and upregulation in gene expression. Conversely, negative Log2FC values indicate hypomethylation in cfMEDIP and downregulation in gene expression. Hyper-up genes refer to those exhibiting a positive correlation between hypermethylation and upregulation, whereas hyper-down genes denote a distinct pattern in which hypermethylation is linked with downregulation. DMG: Differentially methylated gene; DEG: Differentially expressed gene; OC: Ovarian cancer; HBD: Healthy blood donor.

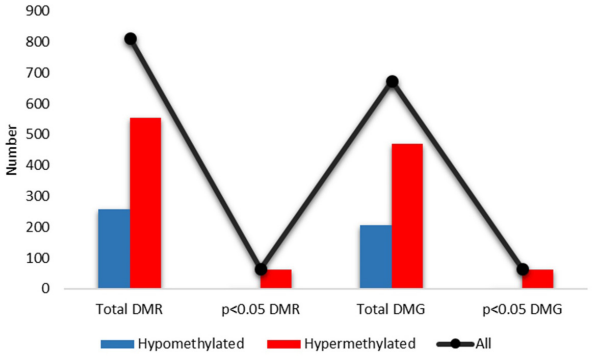

Figure 1. Categorization of DMRs and DMGs.
This figure presents a bar plot illustrating the categorization of DMRs and DMGs based on methylation status. The bars are color-coded, with hypermethylated regions in red and hypomethylated regions in blue. In addition, a black line represents the total number of DMRs and DMGs. DMR: Differentially methylated region; DMG: Differentially methylated gene.

Isolation of cfDNA

For cfDNA isolation, frozen plasma samples were thawed at room temperature, which can cause the presence of cryoprecipitates. To eliminate these substances, plasma samples were centrifuged at 16.000 g for 5 min at 4°C, and the supernatant was carefully transferred to a new tube, avoiding the pellet. This supernatant was then used for cfDNA isolation following the recommended protocol for 4 mL of plasma outlined in the QIAamp® Circulating Nucleic Acid Kit (Qiagen, Catalogue No: 55114, Hilden, Germany). The concentration of isolated cfDNA was measured using a Qubit dsDNA HS Assay Kit (Thermo Fisher Scientific, Catalogue No: Q32851, Waltham, MA, USA) and a Qubit fluorometer (Thermo Fisher Scientific, Waltham, MA, USA). The quality and fragment size distribution of cfDNA were assessed using an Agilent High Sensitivity DNA Reagent Kit (Agilent Technologies, Catalogue No: 5067-4626, Santa Clara, CA, USA) and an Agilent Bioanalyzer (Agilent Technologies, Santa Clara, CA, USA). Specifically, to ensure the integrity of our cfDNA samples, we performed quality control using an Agilent Bioanalyzer after the final library amplification. This assessment confirmed that the final libraries contained only cfDNA fragments with no detectable genomic DNA contamination, thereby validating the effectiveness of our purification process and the high purity of the cfDNA used in our study.

Circulating Cell-Free Methylated DNA Immunoprecipitation

Filler DNA was prepared according to established procedures. A pool of six PCR amplicons, each differ in size and CpG density (1CpG, 5CpG, 10CpG, 15CpG, 20LCpG, and 20SCpG), as originally described by Taiwo et al., were generated (15). Among these, fragments of 1CpG, 5CpGs, 10CpGs, 15CpGs, and 20LCpGs were methylated *in vitro*, whereas the 20SCpG fragment remained unmethylated. A 50:50 ratio of methylated to unmethylated DNA was utilized in the filler DNA mixture, consistent with previous studies. The library preparation protocol using the Kapa Hyper Prep Kit (Roche, Catalogue No: KK8504, Basel, Switzerland) was followed. Briefly, library preparation involves three primary stages: end repair and adenylation, adaptor ligation and purification, and final library amplification. The initial phase of end repair and adenylation was performed according to the protocol. To ensure consistency, the initial cfDNA input for library preparation was standardized at 10 ng per sample. The NEBNext Multiplex Oligos (New England Biolabs, Catalogue No: E7335S, Ipswich, MA, USA) adaptors were customized according to the initial cfDNA concentration and the recommended minimum 100:1 adaptor/insert ratio using the Kapa Hyper Prep Kit. After adaptor ligation, purification was conducted employing AMPure XP beads (Beckman Coulter, Catalogue No: A63881, Brea, CA, USA) by the protocol. Before the immunoprecipitation method, the pool DNA amount (comprising adaptor-ligated cfDNA and filler DNA) was adjusted to 100 ng for all samples, with the initial amount of adaptor-ligated cfDNA set at 10 ng for each sample and the remaining 90 ng supplemented with previously prepared and quantified filler DNA fragments. The 5-mC monoclonal antibody was diluted 1:15 and added to the samples. The immunoprecipitation was carried out following the MagMeDIP Kit (Diagenode, Catalogue No: C02010021, Seraing, Belgium) protocol with pooled cell-free DNA (cfDNA) with lambda DNA and spike-in DNA. Magnetic bead-based washing procedure was executed to expunge non-specifically bound DNA fragments, followed by incubation at 17°C for 4 h. The final libraries were indexed using the NEB index primer set 1 (New England Biolabs, Catalogue No: E7335L, Ipswich, MA, USA) to label individual samples.

Next-Generation Sequencing

The final libraries from all samples were combined in equimolar concentrations to create a pooled library, which was diluted to 4 nM and sequenced using paired-end reads of 150 bp. Library quantification, dilution, and loading were performed according to the manufacturer's instructions. NGS was performed using the Illumina NovaSeq 6000 platform (Illumina, San Diego, CA, USA).

Bioinformatics Analysis

Raw sequencing data from cfMeDIP-seq underwent adapter trimming, low-quality base removal, and filtering using Trimmomatic. Raw sequencing data were normalized using DESeq2 normalization and Methylation Z-score normalization. DESeq2 normalizes raw read counts based on gene length and calculates size factors, which are the median ratios of observed read counts to geometric mean counts across all genes. Normalized read counts were obtained by dividing raw counts by these size factors, adjusting for sequencing

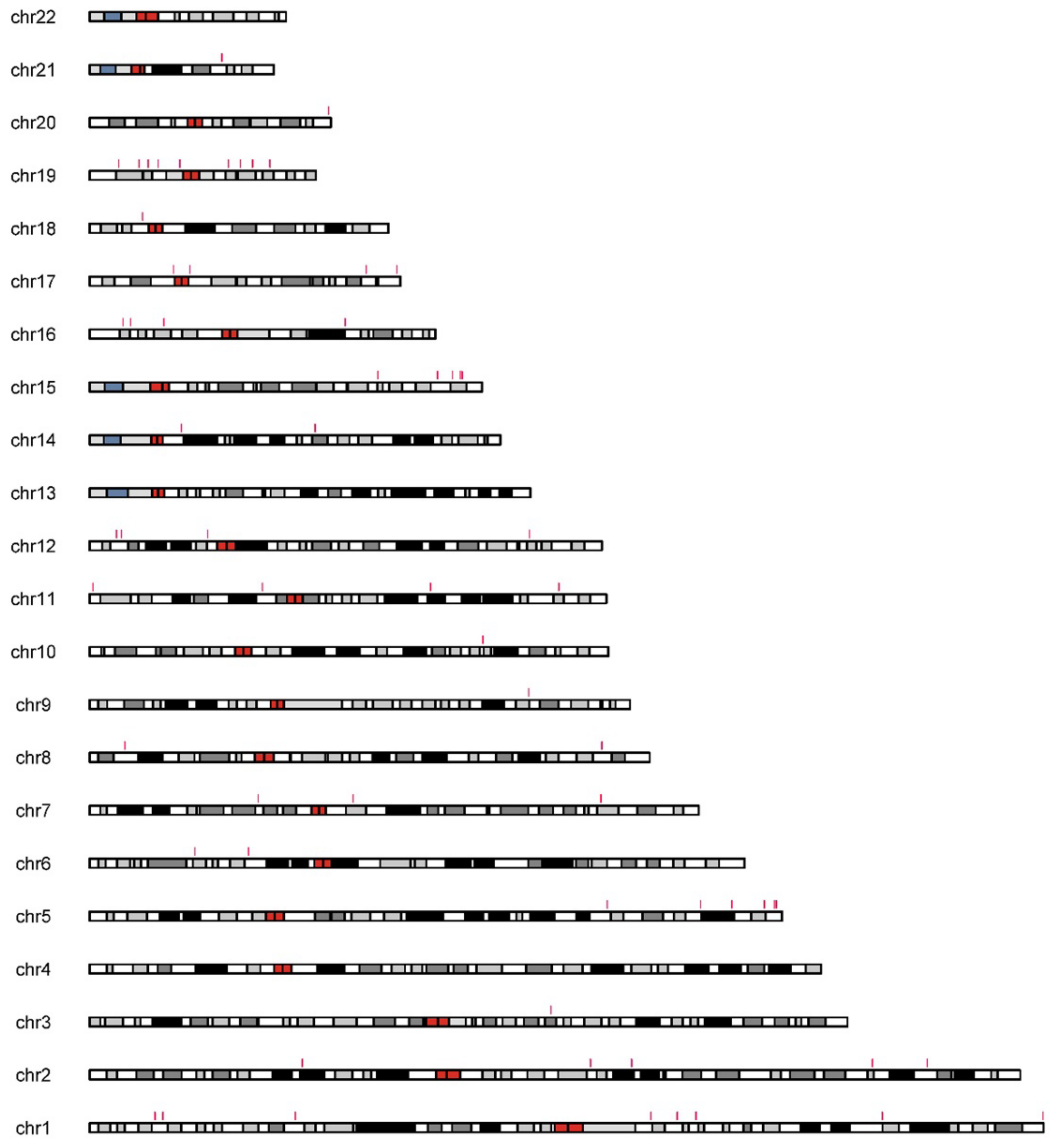

Figure 2. Genomic distribution of DMRs.
This figure presents a chromosome ideogram plot showing the genomic positions of all 64 identified DMRs across the chromosomes. Each DMR is indicated by a red marker along the chromosome, providing insight into the genomic distribution of DNA methylation alterations associated with OC. DMR: Differentially methylated region; OC: Ovarian cancer; chr: Chromosome.

depth, and enabling fair comparisons between samples. Normalized data were aligned to the human reference genome (hg19) using Burrows-Wheeler alignment. DMRs and methylation levels in DMRs relative to the HBDs were determined using DESeq2. Z-score normalization was applied to DESEQ2 normalized data. The method transforms data to have a mean of zero and a standard deviation of one by comparing relative methylation patterns across samples. For each gene, the mean and standard deviation of normalized counts across all samples were calculated, and each count was adjusted by subtracting the mean and dividing by the standard deviation. The analysis focused on 2-kilobase regions around transcription start sites and considered only autosomal chromosomes. The regions without raw data in more than 75% of the samples were excluded. Statistical evaluation of the results involved calculating p values and adjusted p values (q values) using the Benjamini-Hochberg correction in DESeq2. DMRs with a calculated $p<0.05$ were considered significant. The GEPIA2 website (http://gepia2.cancer-pku.cn/#index) was used to obtain a list of differentially expressed genes. Analysis

was performed using the LIMMA method, similar to DESeq2, but was designed for low-density data sets like microarray data. Only genes with a $p<0.05$ were considered significant. To determine the correlation between DMG and DEG levels, Spearman's correlation analysis was performed.

To conduct the survival analysis, we used GEPIA2, which evaluates the relationship between gene expression levels and patient survival based on TCGA data (https://portal.gdc.cancer.gov/). GEPIA2 employs log-rank tests and Cox proportional hazard models to analyze survival outcomes and create survival curves. We analyzed gene expression data from 424 ovarian cancer samples provided by TCGA. The data cover sample collection periods from 1992 to 2014, with survival times ranging from 0 to 180 months, as shown in the survival plots.

Moreover, we assessed the diagnostic potential of 64 DMGs and 18 specific DMG-DEGs by performing Principal Component Analysis (PCA) using GEPIA2. PCA is a statistical technique that simplifies complex datasets by reducing their dimensionality while emphasizing significant patterns. It identifies principal components, which are the directions of greatest variance in the data. By representing the dataset as a linear combination of these components, PCA facilitates the visualization and interpretation of the distinctions between OC tumor and normal ovarian tissues. This analysis utilized transcriptomic data from TCGA ovarian cancer samples to evaluate the efficacy of these DMGs can differentiate between tumor and normal ovary tissue.

Statistical Analyses and Visualization

Visualization of methylation and gene expression profiles was conducted using online tools (https://www.bioinformatics.com.cn/en, http://www.heatmapper.ca/ and http://cancer-pku.cn/). The relationship between methylation level changes in DMRs and expression levels of genes in these regions was analyzed using the nonparametric Spearman correlation test.

RESULTS

In this study, we identified and analyzed DMRs in cfDNA from OC patients compared with HBDs, focusing on elucidating the epigenetic alterations associated with OC. Furthermore, we assessed the effects of DMRs on methylated gene expression using data from TCGA.

Epigenetic Shifts in Ovarian Cancer: Revealing Methylation Dynamics

The cfMeDIP-seq bioinformatics analysis demonstrated that the total number of unique reads for all samples ranged from 5 million to 15 million. This coverage depth is considered sufficient for robust differential analysis using DESeq2. Analysis of cfDNA from OC patients revealed substantial alterations in DNA methylation patterns. A total of 811 DMRs between OC and HBDs were identified, indicating epigenetic dysregulation associated with OC. Among these DMRs, 554 regions exhibited hypermethylation, whereas 257 regions showed hypomethylation in the OC group compared with the controls. Further refinement of the analysis at a significance threshold of $p<0.05$ yielded 64 DMRs (Table 2), with 62 hypermethylated and 2 hypomethylated regions meeting this criterion (Figure 1). We observed that all statistically significant DMRs ($p<0.05$) are in distinct genes across the genome (Figure 2). Only 3% of the DMRs were identified as hypomethylated, whereas 97% of the significant DMRs were hypermethylated (Figure 3).

Characterizing Epigenetic Patterns of Ovarian Cancer

In our exploration of the epigenetic signature in ovarian cancer, we calculated the methylation Z-score for each DMR ($p<0.05$) across all samples. This allowed us to quantitatively assess the methylation status of each DMR relative to the overall methylation pattern in the dataset. Subsequently, visualization of these methylation patterns using a heatmap provided a comprehensive overview of the methylation profiles across samples and DMRs. Hierarchical cluster analysis employing the average linkage method and Spearman rank correlation metrics revealed distinct patterns of methylation similarity or dissimilarity between samples and DMRs (Figure 4). These

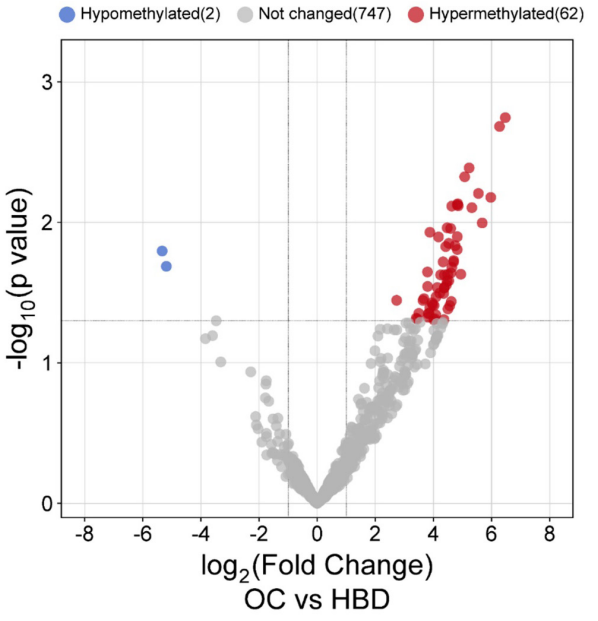

Figure 3. Volcano plot analysis of the DMRs.
This figure displays a volcano plot depicting the statistical significance (p value) and fold change (log2foldchange) of DMRs. DMRs meeting the significance criterion ($p<0.05$) and exhibiting a fold change greater than -1 or less than 1 are highlighted. Hypermethylated and hypomethylated DMRs are represented by red and blue dots, respectively. DMR: Differentially methylated region; OC: Ovarian cancer; HBD: Healthy blood donor.

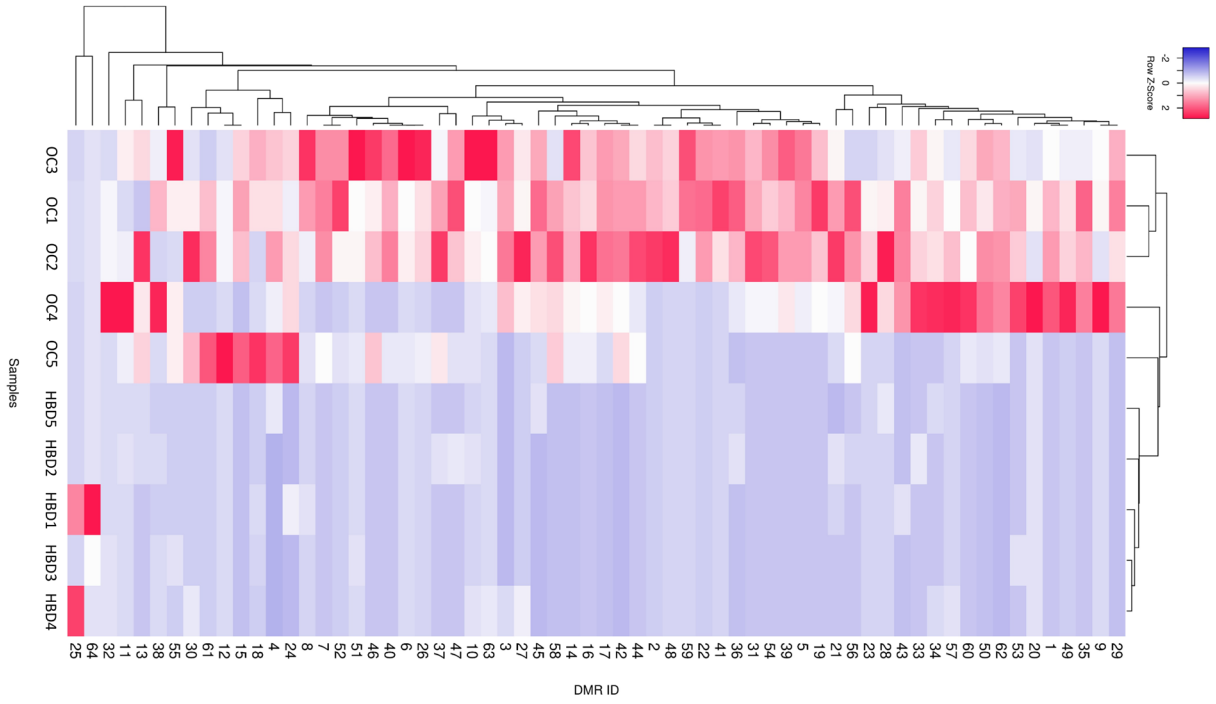

Figure 4. Heatmap of DNA methylation signatures.
Heatmap showing the methylation status of DMRs in OC samples relative to HBDs. Methylation levels are represented on a scale from -2 to 2, with hypermethylation displayed in red and hypomethylation displayed in blue. Using hierarchical cluster analysis with the average linkage method and Spearman rank correlation metrics, the heatmap highlights distinct patterns of methylation alterations in OC and HBDs. OC: Ovarian cancer; HBD: Healthy blood donor; DMR ID: Differentially methylated region identifier.

results provided insights into sample clustering based on epigenetic signatures. As a result, a detailed examination of the clusters in the heatmap revealed a clear and strong correlation within the HBD group, as evidenced by the very short vertical cluster arms on the right side. Additionally, the OC samples were distinctly separated, with a strong correlation among the three OC samples observed on the left side.

Integrative Analysis of DMGs and DEGs in OC

To explore the functional implications of the identified DMRs, we investigated the differentially expressed genes in OC from TCGA data using the GEPIA2 database. We identified 7641 DEGs in TCGA OC tissue samples compared to normal ovarian tissue from genotype-tissue expression (GTEx). We compared our DMGs from cfMEDIP with these DEGs from GEPIA2. This analysis identified 18 genes with overlapping differential methylation and expression patterns in ovarian cancer (Table 3).

Our correlation analysis, employing Spearman's rank correlation, assessed the relationship between methylation status of DMGs and expression level of DEGs in OC samples. A $p<0.05$ was applied to determine statistical significance. The analysis revealed two distinct correlation patterns. Ten genes exhibited a negative correlation between hypermethylation and gene downregulation, indicating a hypermethylation-downregulation relationship. These genes include *PRDM11, CAPRIN2, ATN1, POU5F1P3, NR2F2, DYNC1LI2, LYRM9, FMO5, CCDC88A,* and *UIMC1*. In contrast, eight genes exhibited a positive correlation between hypermethylation and gene upregulation, representing a hypermethylation-upregulation relationship. These genes were *TMC5, SECTM1, NOTCH3, B3GNT3, LINC01224, S100A16, LRP8,* and *WWC1* (Figure 5).

Survival analysis was performed to evaluate the prognostic significance of these 18 overlapping genes. Among them, *B3GNT3*, a hyper-up gene, demonstrated a significant association with overall survival. Additionally, we explored the role of two DMGs identified as cancer driver genes in the COSMIC database. Although the expression of one of these genes, *LRP1B*, was not statistically significant when compared with normal tissues in the OC TCGA dataset, it approached statistical significance for overall survival ($p=0.053$) and was associated with decreased gene expression (Figure 6).

Principal Component Analysis Reveals Distinct Clusters

To further investigate all DMGs and overlapped DMG-DEG, we performed a PCA using GEPIA2. For the first PCA, we used 64

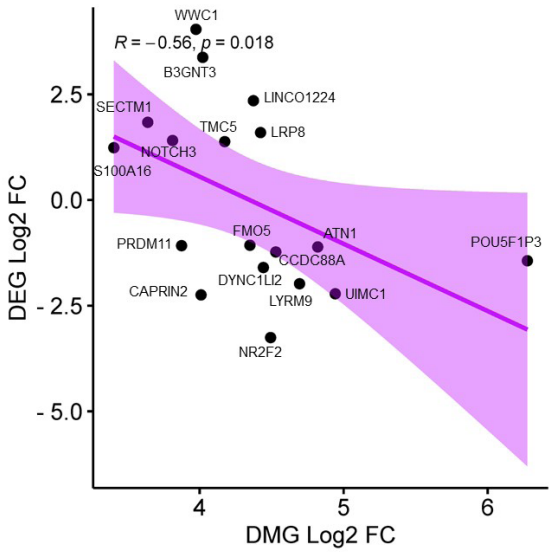

Figure 5. Correlation analysis between DNA methylation and gene expression.
The results of Spearman correlation analysis examining the relationship between levels of DNA methylation and gene expression in OC samples versus HBD. Each data point in the scatter plot represents a gene, with the x-axis indicating the DMG and the y-axis representing the DEG expression level. The negative correlation between DMG and DEG levels is indicated by a downward trend in the scatter plot. The statistical significance of the correlation was assessed using the p value, with values below 0.05 considered significant. DMG: Differentially methylated gene; DEG: Differentially expressed gene; OC: Ovarian cancer; HBD: Healthy blood donor.

DMGs identified in our cfMEDIP analysis. However, only 51 of the DMGs were recognized in the GEPIA2 database. We refined our analysis by focusing on 18 DMGs that overlapped with DEGs identified in GEPIA2, and included 2 additional DMGs from the COSMIC database (*LRP1B* and CD28), resulting in a total of 20 DMGs for the second PCA (Figure 7). In the first PCA analysis, PC1, PC2, and PC3 explained 54%, 9%, and 4% of the variance, respectively. In the second PCA analysis, similar patterns were observed for PC1 (42%), PC2 (18%), and PC3 (8%).

DISCUSSION

Our study provides a comprehensive analysis of DNA methylation alterations in OC by examining cfDNA in plasma samples. By comparing the methylation patterns between OC patients and HBDs, we identified significant epigenetic changes that highlight the potential role of DNA methylation in OC pathogenesis. Using cfDNA isolated from 5 OC patients and 5 HBDs for cfMEDIP-Seq, bioinformatics analysis identified differentially methylated regions (DMRs), revealing significant methylation alterations predominantly in OC samples. Hierarchical clustering and heatmap visualization highlighted distinct methylation patterns in OC and HBDs. Integration with TCGA data identified 18 genes with overlapping methylation and expression changes, with *B3GNT3* emerging as a potential prognostic marker. Additionally, *LRP1B* and CD28 were identified as cancer driver genes in the COSMIC database. These findings underscore the importance of DNA methylation in OC and suggest novel diagnostic and therapeutic strategies.

Our results revealed significant alterations in DNA methylation patterns between OC patients and HBDs, with 62 hypermethylated and 2 hypomethylated DMRs identified. The predominance of hypermethylation events aligns with the established notion that tumor suppressor genes are often silenced by promoter hypermethylation in cancer (16). This silencing can disrupt normal cellular functions, such as cell cycle regulation, apoptosis, and DNA repair, contributing to tumorigenesis (17, 18). The notable predominance of hypermethylated DMRs suggests the potential concerted efforts of cancer cells to silence tumor suppressor genes and activate oncogenes; however, caution is advised in interpreting this bias due to technical constraints. These findings underscore the complexity of DNA methylation alterations in ovarian cancer and provide a foundation for further exploration of their functional implications in disease progression and diagnosis. The distinguish ability of the identified 64 DMGs between OC patients and the HBDs was assessed using Methylation Z-scores obtained from methylation datasets. Heatmap analysis provides valuable insights into how OC and HBDs are clustered based on their epigenetic patterns. Further investigation into the biological implications of these methylation patterns and their association with clinical outcomes in ovarian cancer is warranted.

Our integrative analysis using TCGA dataset revealed 18 genes exhibiting both differential methylation and expression in OC. The majority of these genes demonstrated a negative correlation between methylation and expression levels, consistent with the epigenetic regulation model in which promoter hypermethylation leads to gene silencing. Notably, we identified a subset of ten "hyper-down genes" where hypermethylation correlated with downregulation, supporting their potential role as tumor suppressor genes. Conversely, the remaining eight genes exhibited hypermethylation upregulation patterns, which may indicate complex regulatory mechanisms or context-dependent roles in OC (19).

PCA analysis, which was conducted using both the 64 DMGs and the 20 DMGs overlapping with DEGs or driver gene lists, demonstrated a clear separation between OC samples and normal samples. The OC samples formed distinct clusters in the PCA plots, highlighting significant differences in the DMG-DEG expression profiles. The observed separation underscores the robustness of the identified DMRs and their potential role in differentiating between ovarian cancer and normal ovarian tissue.

Among the DMGs analyzed, *B3GNT3* and *LRP1B* emerged as particularly notable. *B3GNT3* was identified as significant in

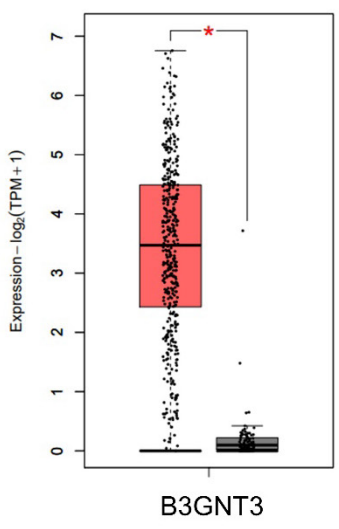

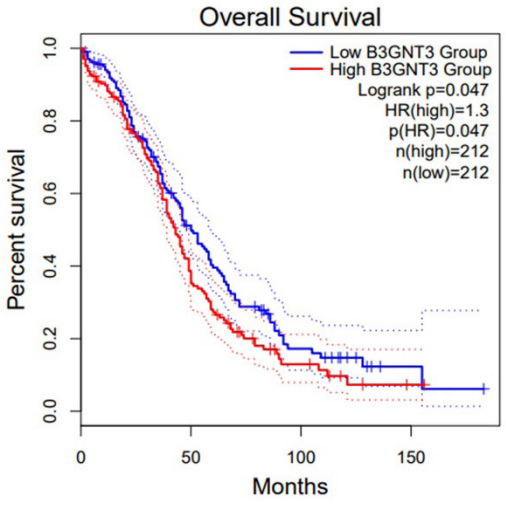

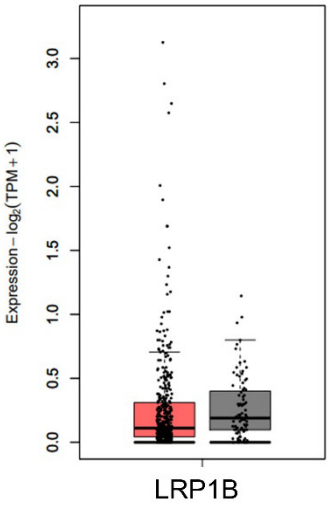

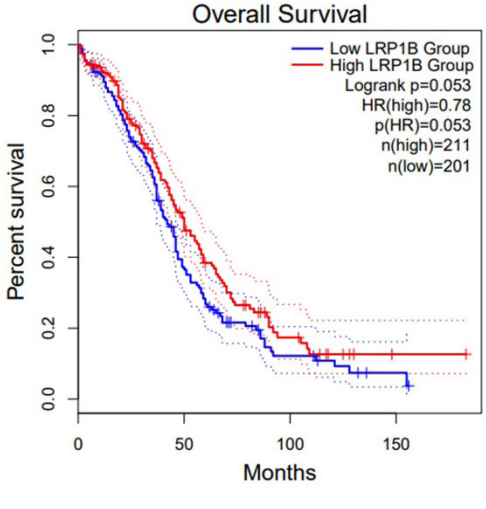

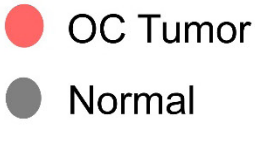

Figure 6. Expression and survival analyses of the B3GNT3 and LRP1B Genes in TCGA.
This figure presents the results of gene expression analysis (left) and survival analysis (right) conducted to assess the expression levels and prognostic significance of two genes, B3GNT3 (top) and LRP1B (bottom), in OC. The left panel displays the gene expression levels of B3GNT3 and LRP1B in OC samples compared with the normal ovarian tissue samples. Expression levels are depicted on the y-axis, with compared groups (legend indicates) on the x-axis. The right panel illustrates the survival analysis results for B3GNT3 and LRP1B in ovarian cancer patients. Kaplan-Meier survival curves depict the overall survival probability over time for patients with high and low expression levels of B3GNT3 and LRP1B. TCGA: The Cancer Genome Atlas; OC: Ovarian cancer.

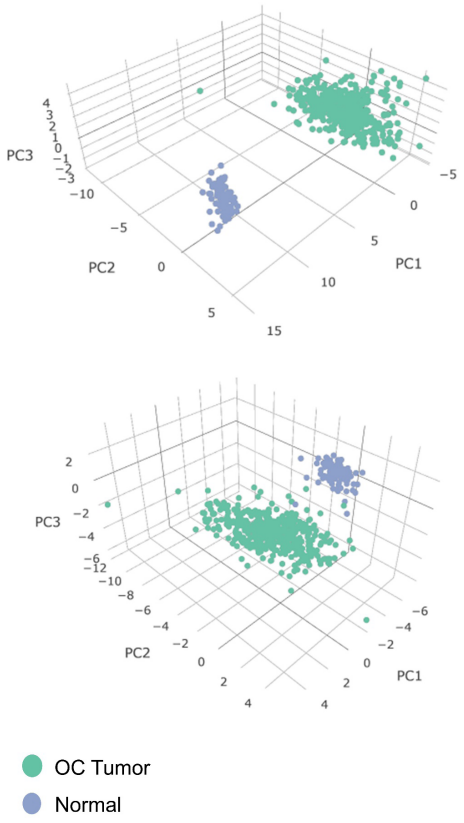

Figure 7. PCA of DMR Signature in TCGA data.
3D PCA plot of the distribution of OC and normal ovarian tissue samples based on DMR signature. The axes of the plot represent the three principal components (PC1, PC2, and PC3), with PCA-1 depicted at the top and PCA-2 at the bottom, capturing the highest variance in the data. In the first PCA, 64 DMGs identified in the cfMEDIP analysis were utilized, while in the second PCA, a refined set of 20 DMGs, including 18 overlapping DEGs identified in GEPIA2 and 2 additional DMGs from the COSMIC database (LRP1B and CD28), were included. The color legend indicates OC and normal ovarian tissue.
PCA: Principal component analysis; DMR: Differentially methylated region; DMG: Differentially methylated gene; DEG: Differentially expressed gene; OC: Ovarian cancer; TCGA: The Cancer Genome Atlas; COSMIC: Catalogue of somatic mutations in cancer.

survival analysis, highlighting its potential as a prognostic marker. *LRP1B*, while nearly significant with a p value close to the threshold, is recognized for its role as a cancer driver gene. We focused on these two genes because of their relevance to survival outcomes, as they exhibited more pronounced associations than other DMGs. However, we acknowledge that other identified genes may have diagnostic value and warrant further investigation.

B3GNT3 is a glycosyltransferase enzyme involved in the glycosylation of proteins, including programmed death-ligand 1 (PD-L1), which plays a role in tumor immune evasion. In certain cancers, the upregulation of B3GNT3 can enhance the glycosylation and stability of PD-L1, contributing to tumor progression by helping tumor cells evade the immune response (20, 21). Moreover, upregulated *B3GNT3* in gynecologic cancers correlates with diagnosis, poor prognosis, immune infiltration, and NF-κB signaling activation, suggesting its role as a carcinogenic factor in these cancers (22). In this study, *B3GNT3* was identified as a hyper-upregulated gene. Its hypermethylation was paradoxically associated with its upregulation and poor survival outcomes, suggesting a potential oncogenic role. This finding is particularly intriguing because it contradicts the typical model in which hypermethylation leads to gene silencing. Instead, it indicates that *B3GNT3* may be activated through alternative regulatory mechanisms in OC.

In contrast, *LRP1B* was identified as a tumor suppressor gene with hypermethylation correlated with its downregulation. Previous studies have implicated *LRP1B* in various cancers, where its loss of function is associated with increased tumorigenicity and metastasis (23, 24). Our results corroborate these findings and highlight the potential of *LRP1B* as a therapeutic target. Restoring *LRP1B* function through demethylating agents or other epigenetic therapies could offer a novel approach for OC treatment.

It is important to acknowledge the limitations of our study, including its relatively small sample size and the need for validation in independent cohorts. Additionally, translating epigenetic findings into clinical practice poses challenges related to standardization of methodologies and integration into existing diagnostic and prognostic frameworks. Addressing these challenges is crucial for realizing the full potential of epigenetic markers in the management of ovarian cancer. Despite these challenges, our findings provide valuable insights into the epigenetic landscape of ovarian cancer and pave the way for further research into personalized therapeutic interventions targeting aberrant DNA methylation.

Ethics Committee Approval: This study was approved in 2020 by Istanbul University, Istanbul Faculty of Medicine Clinical Research Ethics Committee under file number 1451.

Informed Consent: All participants provided voluntary informed consent by completing the consent forms after receiving detailed information.

Peer-review: Externally peer-reviewed.

Author Contributions: Conception/Design of Study – T.S.K., S.T., M.J., T.G.; Data Acquisition – T.S.K., J.H., S.T., M.J.; Data Analysis/Interpretation - T.S.K., J.H., M.J.; Drafting Manuscript – T.S.K., M.J., T.G., J.H., S.T.; Critical Revision of Manuscript - T.S.K., M.J., T.G., S.Topuz.; Final Approval and Accountability – T.S.K., M.J., T.G., J.H., S.T., S.Topuz.

Conflict of Interest: The authors declare no conflict of interest.

Financial Disclosure: This study was supported by the Scientific Research Projects Coordination Unit of Istanbul University, project number 36308.

REFERENCES

1. Feng J, Xu L, Chen Y, Lin R, Li H, He H. Trends in incidence and mortality for ovarian cancer in China from 1990 to 2019 and its forecasted levels in 30 years. J Ovarian Res 2023; 16(1): 139.
2. Balla A, Bhak J, Biró O. The application of circulating tumor cell and cell-free DNA liquid biopsies in ovarian cancer. Mol Cell Probes 2022; 66: 101871.
3. Hinchcliff E, Westin SN, Herzog TJ. State of the science: contemporary front-line treatment of advanced ovarian cancer. Gynecol Oncol 2022; 166(1): 18-24.
4. Roque R, Ribeiro IP, Figueiredo-Dias M, Gourley C, Carreira IM. Current applications and challenges of next-generation sequencing in plasma circulating tumor DNA of ovarian cancer. Biology 2024; 13(2): 88.
5. Giannopoulou L, Mastoraki S, Buderath P, Strati A, Pavlakis K, Kasimir-Bauer S, et al. ESR1 methylation in primary tumors and paired circulating tumor DNA of patients with high-grade serous ovarian cancer. Gynecol Oncol 2018; 150(2): 355-60.
6. Lu H, Liu Y, Wang J, Fu S, Wang L, Huang C, et al. Detection of ovarian cancer using plasma cell-free DNA methylomes. Clin Epigenetics 2022; 14(1): 74.
7. Margolin G, Petrykowska HM, Athamanolap P, Goncearenco A, Osei-Tutu A, Annunziata CM, et al. Leveraging locus-specific epigenetic heterogeneity to improve the performance of blood-based DNA methylation biomarkers. Clin Epigenetics 2020; 12: 154.
8. Marinelli LM, Kisiel JB, Slettedahl SW, Mahoney DW, Lemens MA, Shridhar V, et al. Methylated DNA markers for plasma detection of ovarian cancer: discovery, validation, and clinical feasibility. Gynecol Oncol 2022; 165(3): 568-76.
9. Peng S, Zhang X, Wu Y. Potential applications of DNA methylation testing technology in female tumors and screening methods. Biochim Biophys Acta Rev Cancer 2023; 1878(5): 188941.
10. Papanicolau-Sengos A, Aldape K. DNA methylation profiling: an emerging paradigm for cancer diagnosis. Annu Rev Pathol 2022; 17: 295-321.
11. Asante D-B, Calapre L, Ziman M, Meniawy TM, Gray ES. Liquid biopsy in ovarian cancer using circulating tumor DNA and cells: ready for prime time? Cancer Lett 2020; 468: 59-71.
12. Govindarajan M, Wohlmuth C, Waas M, Bernardini MQ, Kislinger T. High-throughput approaches for precision medicine in high-grade serous ovarian cancer. J Hematol Oncol 2020; 13: 1-20.
13. Sánchez-Herrero E, Serna-Blasco R, Robado de Lope L, González-Rumayor V, Romero A, Provencio M. Circulating tumor DNA as a cancer biomarker: an overview of biological features and factors that may impact on ctDNA analysis. Front Oncol 2022; 12: 943253.
14. Li Y, Fan Z, Meng Y, Liu S, Zhan H. Blood-based DNA methylation signatures in cancer: a systematic review. Biochim Biophys Acta Mol Basis Dis 2023; 1869(1): 166583.
15. Taiwo O, Wilson GA, Morris T, Seisenberger S, Reik W, Pearce D, et al. Methylome analysis using MeDIP-seq with low DNA concentrations. Nat Protoc 2012; 7(4): 617-36.
16. Geissler F, Nesic K, Kondrashova O, Dobrovic A, Swisher EM, Scott CL, et al. The role of aberrant DNA methylation in cancer initiation and clinical impacts. Ther Adv Med Oncol 2024; 16: 17588359231220511.
17. Chen YC, Elnitski L. Aberrant DNA methylation defines isoform usage in cancer, with functional implications. PLoS Comput Biol 2019; 15(7): e1007095.
18. Rini BI, Zhang J, Hall O, Bergener J, Wang Y, Brown B, et al. 1910P evaluation of a genome-wide methylome enrichment platform for circulating tumor DNA quantification and prognostic performance in renal cell carcinoma (RCC). Ann Oncol 2023; 34: S1028.
19. Rauluseviciute I, Drabløs F, Rye MB. DNA hypermethylation associated with upregulated gene expression in prostate cancer demonstrates the diversity of epigenetic regulation. BMC Med Genomics 2020; 13(1): 6.
20. Ren X, Lin S, Guan F, Kang H. Glycosylation targeting: a paradigm shift in cancer immunotherapy. Int J Biol Sci 2024; 20(7): 2607-21.
21. Leng X, Wei S, Mei J, Deng S, Yang Z, Liu Z, et al. Identifying the prognostic significance of *B3GNT3* with PD-L1 expression in lung adenocarcinoma. Transl Lung Cancer Res 2021; 10(2): 965.
22. Xu J, Guo Z, Yuan S, Li H, Luo S. Upregulation of *B3GNT3* is associated with immune infiltration and activation of NF-κB pathway in gynecologic cancers. J Reprod Immunol 2022; 152: 103658.
23. Príncipe C, Dionísio de Sousa IJ, Prazeres H, Soares P, Lima RT. LRP1B: a giant lost in cancer translation. Pharmaceuticals 2021; 14(9): 836.
24. Cowin PA, George J, Fereday S, Loehrer E, Van Loo P, Cullinane C, et al. *LRP1B* deletion in high-grade serous ovarian cancers is associated with acquired chemotherapy resistance to liposomal doxorubicin. Cancer Res 2012; 72(16): 4060-73.